

THE INVESTIGATION OF THE IMPROVED PROPERTIES OF  
N<sup>+</sup>-IMPLANTED AMORPHOUS BRIGHT CHROMIUM DEPOSITED  
(ABCD) ELECTROPLATE

By

CHARLES K. MOUNT

A DISSERTATION PRESENTED TO THE GRADUATE SCHOOL  
OF THE UNIVERISTY OF FLORIDA IN PARTIAL FULFILLMENT  
OF THE REQUIREMENTS FOR THE DEGREE OF  
DOCTOR OF PHILOSOPHY

UNIVERSITY OF FLORIDA

1997

Copyright 1997

by

Charles K. Mount

This dissertation is dedicated to the memory of H. A. Laitinen.

## ACKNOWLEDGMENTS

I appreciate the exposure to a better outlook on life, good science, fine wine and GVAR that I received from Gar Hoflund. The lessons will not be lost. I also appreciate Bob Ben, Ed Cooper and the denizens of The Market Street Pub for providing unending entertainment during my time as a graduate student.

## TABLE OF CONTENTS

	<u>page</u>
ACKNOWLEDGMENTS	iv
ABSTRACT	vi
CHAPTERS	
1 INTRODUCTION	1
2 NOVEL CHROMIUM LAYERS FORMED BY NITROGEN-ION IMPLANTATION OF CONVENTIONAL AND ABCD ELECTRODEPOSITED FILMS	4
Experimental	4
Results and Discussion	5
Summary	9
3 MODIFICATION OF AMORPHOUS BRIGHT CHROMIUM DEPOSITED (ABCD) FILMS BY NITROGEN ION IMPLANTATION	18
Experimental	18
Results and Discussion	19
4 PREPARATION AND CHARACTERIZATION STUDY OF NITROGEN-ION-IMPLANTED CONVENTIONAL CHROMIUM PLATINGS	28
Experimental	28
Results and Discussion	29
5 CHARACTERIZATION STUDY OF NITROGEN-ION- IMPLANTED AMORPHOUS BRIGHT CHROMIUM DEPOSITED FILM	43
Experimental	43
Results and Discussion	44
6 CONCLUSION	53
Summary and Conclusion	53
Future Investigations	54
REFERENCES	56
BIOGRAPHICAL SKETCH	58

Abstract of Dissertation Presented to the Graduate School  
of the University of Florida in Partial Fulfillment of the  
Requirements for the Degree of Doctor of Philosophy

THE INVESTIGATION OF THE IMPROVED PROPERTIES OF  
N<sup>+</sup>-IMPLANTED AMORPHOUS BRIGHT CHROMIUM DEPOSITED  
(ABCD) ELECTROPLATE

By

Charles K. Mount

December 1997

Chairman: Gar B. Hoflund  
Major Department: Chemical Engineering

Amorphous bright chromium deposits (referred to as the ABCD method) offer significant improvement over conventional chromium electroplate in that they have fewer defects, have smoother surfaces, are more resistant to corrosion and are harder. The hardness of the ABCD electroplate can be significantly increased by various treatments such as annealing and N<sup>+</sup> implantation. This work investigates and compares the improvements obtained by N<sup>+</sup> implantation of ABCD electroplate with that of conventional chromium electroplate and correlates changes in hardness with structure and chemical properties. Implantation leads to increased hardness, but the extent is most pronounced for conventional films which were not annealed and ABCD films which were annealed at or below 400°C for 1/2 h. Using Knoop hardness measurements in a differential manner, it was determined that the near surface region preferentially increases in hardness over the bulk of the electroplate after N<sup>+</sup> implantation. Implantation at high dosages results in the implantation region Cr being bound as CrN, oxides and nitrides with N displacing C in ABCD films. Increased dosages result in decreased N retention values while implanting at

elevated temperatures increases the retained N, causes N to migrate more deeply into the bulk, and yields high hardness values. The effect of annealing ABCD  $N^+$ -implanted films was also examined. A non-annealed film and a 600°C annealed film were  $N^+$ -implanted and characterized using Auger electron spectroscopy (AES), electron spectroscopy for chemical analysis (ESCA or XPS) and X-ray diffraction (XRD). The annealed film is more highly crystalline than the non-annealed film. Diffraction lines due to  $Cr_7C_3$  and  $Cr_2N$  are readily apparent. Auger electron spectroscopy and ESCA show that the film compositions are similar but that the chemical states of the surface species differ in that most of the organic carbon contained in the film is converted to carbide during annealing. These differences are responsible for the increase in Knoop hardness (1660 to 2980) derived from annealing the sample prior to implantation. In pre-annealed ABCD films, the ESCA, AES and XRD data show that the increased hardness is due to an enhanced crystallinity caused by annealing and the concurrent formation of  $Cr_7C_3$ . The  $N^+$  implantation process itself apparently is not affected by the preannealing step. Conventional  $N^+$ -implanted chromium films were also investigated using ESCA (or XPS), AES, depth profiling and ISS to provide a reference for comparison of ABCD electroplate.

## CHAPTER 1 INTRODUCTION

Chromium is a technologically important plating material because its surface retains a high polish, it has desirable mechanical properties and it is resistant to corrosion. Therefore, Cr is widely used as thin-film coatings, prepared by electroplating or chromizing, either to protect the underlying metal or to beautify the surface. Electroplated Cr films are generally classified as decorative or hard. Decorative Cr plating varies between 0.00001 and 0.00002 inch in thickness and is usually deposited over a Ni coating. Hard Cr plating is used in applications requiring high wear resistance and a low coefficient of friction.

A method was developed by Sargent [1] and Fink [2] during the 1920s for electroplating conventional Cr films using a sulphate catalyst. These Cr films are bright and retain their brightness indefinitely. This is important because it eliminates a polishing step, which is usually more costly than the plating step. The Sargent bath conditions produce a very clean initial surface for plating so excellent adhesion is obtained readily in nearly all applications. The fact that surface defects in the base metal are filled-in during electroplating also results in smooth surfaces. These favorable characteristics immediately led to the adoption of combination Ni-Cr and Cu-Ni-Cr plates in the automotive and appliance industries as decorative coatings. There are several difficulties with conventional Cr layers but one of the most severe is that the hardness of these layers decreases as the annealing or operating temperature increases. In 1986 Hoshino *et al.* [3] described a new method for electrodepositing amorphous bright chromium deposits (referred to as the ABCD method) from chromic acid solutions containing organic species with -CHO or -COOH groups. These films are superior to conventional films in that they have fewer defects, have smoother surfaces [4], are more resistant to corrosion by HCl solutions and,



most importantly, have greatly increased hardness at elevated temperatures. The Vicker's hardness of conventional and ABCD films is shown in Fig. 2-1(a) as a function of annealing temperature (for a 1 h annealing period). The hardness of the conventional film decreases monotonically from an as-deposited hardness of 850 to 400 at 800°C. The hardness of the as-deposited ABCD film is 950. It increases slowly to 1200 at 300°C and then rises rapidly to a maximum of 1700 at 500°C before decreasing to 1100 at 800°C. The time dependence of hardness during annealing at various temperatures is shown in Fig. 2-1(b) [5]. This figure shows that a very high hardness is obtained by annealing even at temperatures as low as 200°C for 48 h. Annealing at 300-600°C results in an increase in hardness (above 1600) within a shorter annealing period (1-3 h). Annealing at 700°C results in a fairly rapid (6 h) decrease in hardness to below 1000. The time-dependent annealing behavior of conventional Cr layers also has been examined. Within 12 h of annealing at the various temperatures, the following long-term hardness values are obtained: 800 at 200°C, 800 at 300°C, 800 at 400°C, 600 at 500°C, 350 at 600°C and 350 at 700°C. Both ABCD [4,6,7] and conventional Cr films [4,8] have been examined using several surface analytical techniques.

Rutherford backscattering (RBS) and nuclear reaction analysis (NRA) measurements indicate that the ABCD films contain about 10 at.% C, 5 at.% O and 10 at.% H [H. Baumann, personal communication, 1990]. These films can be grown to thicknesses of many microns and are superior to conventional Cr films in that they have fewer defects and smoother surfaces. Most importantly, the hardness of ABCD films increases monotonically during annealing over the temperature range from 200 to 600°C. Annealing at still higher temperatures results in a decrease in hardness.

The properties of ABCD layers have been examined in several studies [3,6,7] using various techniques. Tsai and Wu [9] have prepared ABCD layers and examined the annealed films using TEM. Their results indicate that the unusual hardness of the films annealed below 600°C is related to a uniform distribution of submicron Cr dispersoids

within a C-rich matrix. Annealing at higher temperatures results in formation of  $\text{Cr}_7\text{C}_3$  and growth of the metal grains. The hardening mechanism is not yet fully understood and questions still remain about the role of carbide formation. It is clear that the properties of annealed ABCD coatings are potentially important with regard to industrial applications in pronounced wear situations at elevated temperatures. The technique of ion implantation has proven to be a useful tool for the modification of steel [10] and Cr surfaces [5,11-13] by increasing microhardness and improving wear rates. These improved properties are due to the formation of hard nitrides and the introduction of internal stresses into the implanted layers.

The purpose of this work is to determine the effect of  $\text{N}^+$  implantation on the hardness of ABCD films and relate the changes to structure and chemistry as compared to chromium electroplated films. The results will then be used for further optimization of ABCD films.

## CHAPTER 2

### NOVEL CHROMIUM LAYERS FORMED BY NITROGEN-ION IMPLANTATION OF CONVENTIONAL AND ABCD ELECTRODEPOSITED FILMS

In this chapter, conventional and ABCD Cr films have been  $N^+$  implanted and the hardness behavior of the films characterized. The compositions of the films as a function of depth have been examined using Auger electron spectroscopy (AES) in conjunction with ion sputter depth profiling.

#### Experimental

Conventional films were prepared using typical Sargent bath conditions [1,2], and ABCD films were prepared using conditions described previously by Hoshino *et al.* [3]. Some of the films were annealed at various temperatures in a mechanically pumped  $10^{-5}$  Torr vacuum for 1 h. The ion implantation was carried out using 90 keV  $N^+$  for conventional layers and 80 keV  $N^+$  for ABCD layers. Although the total dose could be varied, a low flux was used in order to minimize heating of the sample surface region during implantation. It was not possible to measure the sample temperature during implantation, but it is estimated that the sample temperature remained below 250°C.

In previous studies [3,5] Vicker's hardness tests were used to assess mechanical hardness. In this study Knoop hardness tests were carried out instead of Vicker's hardness tests. The Knoop tester has a differently shaped stylus and the load can be varied. Both of these facts allow for variation of the depth sensitivity of the hardness. By using lower loads, the test becomes more surface sensitive. From the measured diameter of the imprint produced using light loads (10 mN), it is estimated that the hardness is primarily characteristic of the properties of the outermost 2000 Å of the Cr layer. This is fortunate because this is approximately the thickness of the implanted layer as described below. It is

not possible to obtain higher surface sensitivity with this technique because the imprints cannot be observed when lighter loads are used.

Compositional depth profiling was performed using both AES in a Perkin-Elmer PHI 550 vacuum system and ESCA in a Kratos XSAM 800 system. The profiles obtained are essentially identical, so only the AES results are presented. Ion sputtering was carried out using a rastered (7 mm x 7 mm) 4 keV Ar ion beam, and the sputter rate is assumed to be that obtained from Ta<sub>2</sub>O<sub>5</sub> standards. This is probably within 10% of the actual sputter rate based on simulation of the implanted layers.

### Results and Discussion

The hardness of N<sup>+</sup>-implanted conventional Cr films (unannealed) as a function of total dose and load is shown in Fig. 2-2. For both the non-implanted and implanted films, the hardness increases as the load decreases, indicating that the near-surface region has a higher hardness than the bulk. The smallest increase in hardness occurs for the non-implanted sample. A surface characterization study of conventional Cr layers [8] shows that the surface of an unannealed film consists of a fairly thick oxidic layer. The hardness result of Fig. 2-2 suggests that this oxidic layer is a little harder than the underlying bulk Cr metal. This is unexpected since oxides typically are not very hard compared to metals. The other curves shown in Fig. 2-2 were all taken from N<sup>+</sup>-implanted samples and exhibit a very high hardness near the surface compared to the bulk values. Furthermore, the near-surface hardness goes through a maximum at an implanted concentration of  $9.3 \times 10^{17}$  N<sup>+</sup> cm<sup>-2</sup>, indicating that an optimum total dose exists for a given sample and implantation conditions. Apparently, the implanted N provides a beneficial effect until so much has been implanted in the near-surface region that the structure of the film becomes disrupted, causing a decrease in hardness. An AES depth profiling spectrum obtained from the optimally implanted Cr samples is shown in Fig. 2-3. The predominant constituents of the film are O, Cr and N, and the outermost layer of the film is an oxide layer, as observed

previously [8]. The N exhibits a broad profile within the outermost 2500 Å, with a maximum of ~33 at.% at a depth of 700 Å. If the sample receives a larger dose of N<sup>+</sup>, the maximum N at.% does not increase above that observed in Fig. 2-3, but the width of the peak maximum region increases. The composition of chromium nitride is CrN, which would correspond to 50 at.% N if all of the Cr in the region of the peak maximum was converted to CrN. However, a significant amount of the Cr would be bonded to the O located in this region. Furthermore, quantification of AES data is quite difficult in this case because the Cr and O peaks overlap and the various chemical states of Cr (metallic, oxidic and probably the nitride) have largely varying peak shapes, which would affect sensitivity factors. Some of the factors pertaining to quantification of O/Cr systems have been discussed by Siconolfi and Frankenthal [14]. Therefore, it is reasonable to consider that the atomic percentages shown in AES depth profiles are only semi-quantitative but that the variational trends in composition with depth and from one sample to another are meaningful. These statements, coupled with the fact that a larger dose does not yield a higher N concentration, suggest that all of the Cr in the most heavily nitrated region is present either as Cr oxides or CrN. A few per cent of C and S are also present in this layer [8].

The hardnesses of ABCD films which were annealed at various temperatures in a mechanically pumped 10<sup>-5</sup> Torr vacuum for 1 h and then N<sup>+</sup>-implanted with 80 KeV ions have been measured using loads of 10, 25 and 50 mN. The hardness values (Knoop) obtained from both non-implanted and implanted ABCD films are shown in Figs. 2-4 and 2-5 as a function of annealing temperature and load. The more surface-sensitive hardness results (10 mN load) are shown in Fig. 2-4 for the N<sup>+</sup>-implanted ABCD samples and non-implanted ABCD samples. For the non-implanted samples the hardness increases monotonically with annealing temperature to 700°C. This is surprising since Fig. 2-1(a) shows that the maximum hardness occurs at an annealing temperature below 700°C. However, the hardness is increasing less rapidly between 600 and 700°C in Fig. 2-4 and would probably go through a maximum at 700°C if higher annealing temperatures were

used. The overall increase in the surface-sensitive hardness with annealing temperature from 20 to 700°C is quite large, ranging from 1250 to 3300.

An important observation is that the hardness of implanted ABCD films is greater than that of non-implanted ABCD films for all annealing temperatures examined, but the difference is much greater at the lower annealing temperatures. Similar to the non-implanted films, the hardness of the implanted films increases with annealing temperature. However, the increase is not as great as that of non-implanted films; 2750-3500 at 20-700°C. The hardness of the 100°C-annealed ABCD is anomalously high owing to an error in setting the total dose during implantation. The other four implanted ABCD films received a dose of  $\sim 7.5 \times 10^{17} \text{ N}^+ \text{ cm}^{-2}$ , but the 100°C-annealed ABCD film received a dose of  $4.0 \times 10^{17} \text{ N}^+ \text{ cm}^{-2}$ . The fact that the hardness of the 100°C ABCD film is abnormally high after receiving a lower dose than the other ABCD films indicates that a dose of  $7.5 \times 10^{17} \text{ N}^+ \text{ cm}^{-2}$  is not optimal and that lower doses would most likely result in greater hardnesses of all the films.

The difference ( $\Delta$ ) curves for the implanted and non-implanted films shown in Fig. 2-4 were obtained by subtracting the hardness obtained using a 25 mN load from the hardness obtained using a 10 mN load. A large  $\Delta$  indicates that the surface region is much harder than the underlying region. The  $\Delta$  curves are similar above 300°C and have a positive slope. This implies that the near-surface layers are becoming preferentially harder with increased annealing temperature and that this occurs primarily due to annealing. Below 300°C the implantation results in much harder near-surface regions compared to the underlying layers. Again, the  $\Delta$  value for the 100°C-annealed and implanted ABCD film appears to be anomalously high.

Similar hardness curves obtained from the same samples using a 50 mN load are shown in Fig. 2-5 for implanted and non-implanted films. These more bulk-sensitive hardness values are considerably lower than the corresponding surface-sensitive values shown in Fig. 2-4 for all cases. Both hardness curves increase monotonically with

annealing temperature in Fig. 2-5, but the overall increase in hardness with increasing annealing temperature is much greater for the non-implanted ABCD films than for the implanted ABCD films. Below 500°C, N<sup>+</sup> implantation very significantly improves the more bulk-sensitive hardness of the ABCD films. At and above 500°C, the more bulk-sensitive hardness values of the non-implanted and implanted ABCD films are identical, indicating that annealing at these temperatures is responsible for determining the hardness.

The difference ( $\Delta$ ) curves for the implanted and non-implanted ABCD films were obtained by subtracting the hardness obtained using a 50 mN load from the hardness obtained using a 25 mN load. The bulk-sensitive and surface-sensitive  $\Delta$  curves for the non-implanted films are nearly identical, indicating that changes in their hardness with depth are uniform. However, the  $\Delta$  curve corresponding to the bulk-sensitive hardness of the implanted ABCD films is lower than the more surface-sensitive  $\Delta$  curve, and it decreases towards zero above 300°C. These facts indicate that the subsurface layers of the implanted ABCD films are more uniform with regard to hardness than the non-implanted films.

Typical AES depth profiling results obtained from implanted ABCD films are shown in Fig. 2-6. These data were taken from an implanted ABCD film that was annealed at 500°C, but they are quite similar to profiles taken from implanted ABCD films annealed at other temperatures. There are considerable differences between these data and the depth profiling data obtained from the implanted conventional film shown in Fig. 2-3. In this case the primary constituents are Cr, N and C. A C-contaminated oxide layer was removed from the film during a presputter period after which the N and Cr signals increased and the C signal decreased. The high concentration of C found in the ABCD films and the low concentration of C found in the conventional Cr films are consistent with the results of the previous characterization studies [4,6-8].

Most of the N is contained within the outermost 1600 Å, and the distribution is quite broad with a maximum of ~40 at.%. This is ~5% higher than the maximum found in

Fig. 2-2 and may be due to a lower concentration of O in the ABCD films, thereby allowing for more of the Cr to be bound as CrN. Throughout this region the Cr signal is essentially constant at ~47 at.%. The N and C profiles in this region are most interesting in that they mimic each other in an inverse manner, i.e. the C concentration is low when the N concentration is high, and vice versa. The shape of the N (C) profile is unusual in that it exhibits two maxima (minima) at the front and rear of the implanted region. This is not the case when a lower N dose is used, as shown in Fig. 2-7. Here, a single maximum is observed in the N profile, and the C profile exhibits a minimum at this same depth. As the retained dose increases, the lobes develop on the N and C profiles. It appears that the N competes more effectively for the Cr than the C, thereby pushing the C into other regions of the film. This assertion explains the fact that N-implanting ABCD films annealed above 500°C provides only a small increase in the more surface-sensitive hardness, as shown in Fig. 2-4. The presence of either C or N increases the hardness of these films, but the presence of both does not significantly alter the hardness because they compete with each other to bond with the Cr. However, more recent experiments demonstrate that very large increases in hardness can be obtained by N<sup>+</sup>-implanting ABCD films at elevated temperatures (> 500°C). This will be discussed further in another chapter.

### Summary

Nitrogen ion implantation (sample temperature < 250°C) of both conventional Cr and ABCD films results in an increase of the near-surface hardness of the Cr layers. The extent of this increase is greatest for conventional films and ABCD films which have been pre-annealed at or below 400°C. The implanted layer extends over the outermost 2000 Å and has a maximum N concentration of 35-40 at.% based on semi-quantitative AES depth profiling results. Increasing the total N dose alters the N profile by increasing the width of the region where the N concentration is maximal. In agreement with previous studies, ABCD films contain much more C than conventional films. During implantation the N



displaces the C in the implanted region to form CrN. Thus, the N and C profiles are inversely related, i.e. the C concentration is low when the N concentration is high, and vice versa. The presence of either N as CrN or C as Cr carbides provides improved hardness, but the presence of both results in a minimal increase in hardness. However, procedures other than those used in this chapter for carrying out the implantation and annealing steps do significantly increase the hardness of ABCD films. These procedures will be described later.

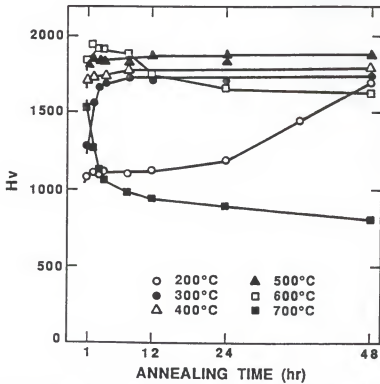
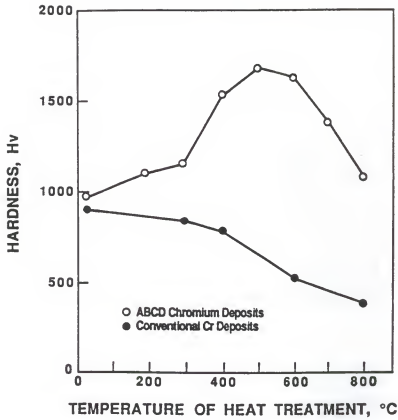


Figure 2-1. (a) Hardness (Vicker's) of conventional Cr and ABCD films annealed for 1/2 h in a  $10^{-5}$  Torr vacuum at various temperatures. (b) Hardness of ABCD films as a function of time while annealing at various temperatures (obtained from [5]).

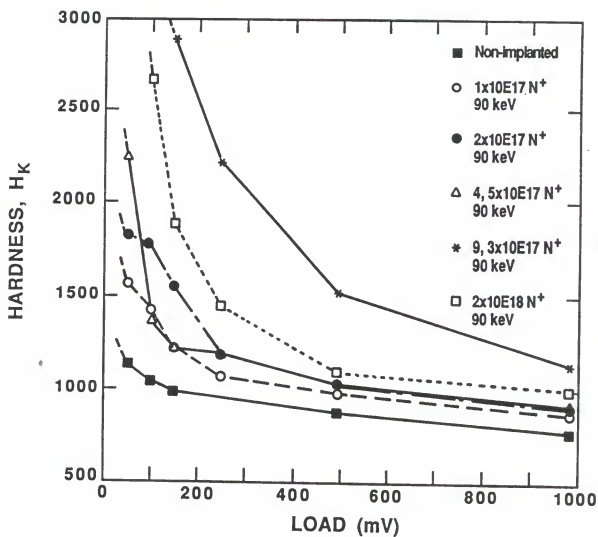


Figure 2-2. Hardness (Knoop) of  $\text{N}^+$ -implanted conventional Cr films (unannealed) as a function of load and total dose ( $\text{N}^+ \text{ cm}^{-2}$ ).

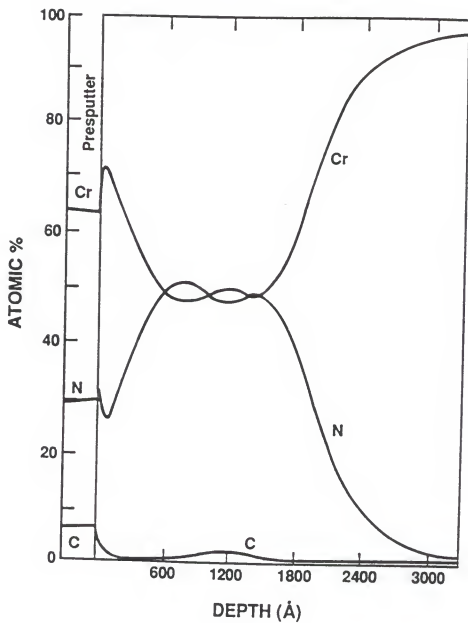


Figure 2-3. Auger depth profile taken from the optimally  $N^+$ -implanted conventional Cr sample showing the film composition as a function of depth. Only the most prominent features due to Cr, O and N have been considered in this analysis.

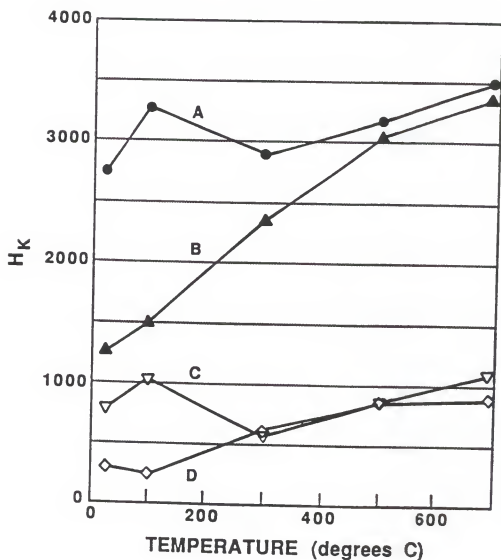


Figure 2-4. Hardness (Knoop) values obtained using a 10 mN load from (A) implanted and (B) non-implanted vacuum-annealed ABCD films. The films were implanted with a dose of  $7.5 \times 10^{17} \text{ N}^+ \text{ cm}^{-2}$  (80 keV) except for the 100°C-annealed film, which was implanted with a dose of  $4.0 \times 10^{17} \text{ N}^+ \text{ cm}^{-2}$ . The difference ( $\Delta$ ) curves shown in (C) implanted and (D) non-implanted films were obtained by subtracting the hardness obtained using a 25 mN load from that obtained using a 10 mN load.

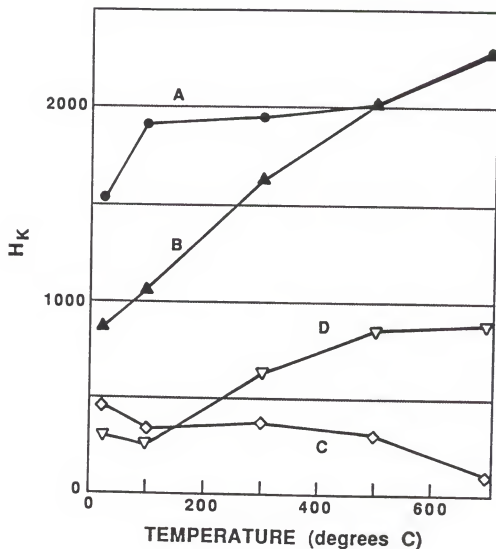


Figure 2-5. Hardness values (Knoop) obtained using a 50 mN load from (A) implanted and (B) non-implanted vacuum-annealed ABCD films. The films were implanted with a dose of  $7.5 \times 10^{17} \text{ N}^+ \text{ cm}^{-2}$  (80 keV) except for the 100°C-annealed film, which was implanted with a dose of  $4.0 \times 10^{17} \text{ N}^+ \text{ cm}^{-2}$ . The difference ( $\Delta$ ) curves shown in (C) implanted and (D) non-implanted films were obtained by subtracting the hardness obtained using a 50 mN load from that obtained using a 25 mN load.

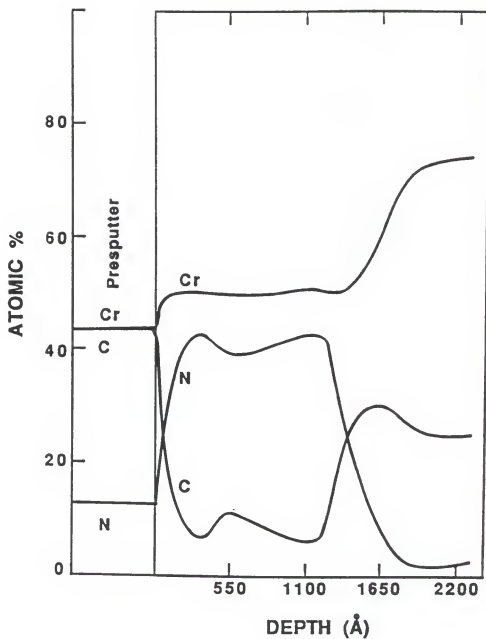


Figure 2-6. Auger depth profile taken from the ABCD sample annealed at 500°C and implanted with a dose of  $8 \times 10^{17} \text{ N}^+ \text{ cm}^{-2}$ . Only the most prominent features due to Cr, N and C have been considered in this analysis.

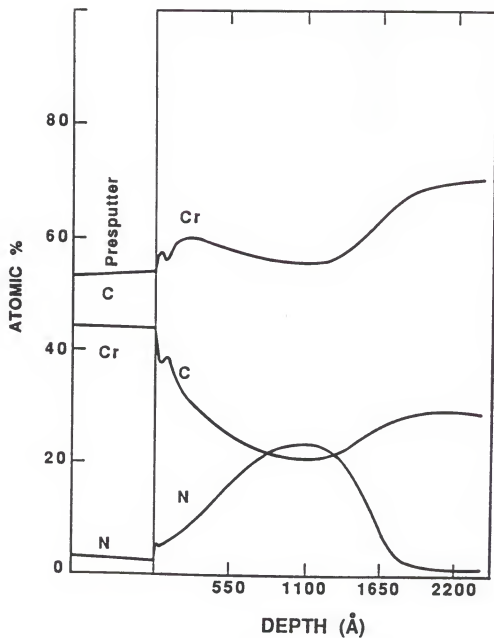


Figure 2-7. Auger depth profile taken from the ABCD sample annealed at 100°C and implanted with a dose of  $4 \times 10^{17} \text{ N}^+ \text{ cm}^{-2}$ . Only the most prominent features due to Cr, N and C have been considered in this analysis.



### CHAPTER 3

#### MODIFICATION OF AMORPHOUS BRIGHT CHROMIUM DEPOSITED (ABCD) FILMS BY NITROGEN ION IMPLANTATION

In the present chapter, the dependence of microhardness and retained N dose in implanted ABCD films on implantation parameters including total dose (fluence), ion energy and implantation temperature has been more closely evaluated. As-deposited as well as pre-annealed samples were used to separate implantation hardening effects from annealing hardening in the beam. Hot implantations (above 500°C) were also carried out.

Sputter depth profiling combined with Auger electron spectroscopy (AES) has been used to characterize the implantation profiles and chemical composition of the implanted films. Penetration depths determined from the Auger data have been compared with the results of transport of ions in matter (TRIM) simulations. Nuclear reaction analysis (NRA) was used to provide a calibration of the Auger data with regard to the total N content of the implanted films. Then AES N depth profile areas were used to evaluate retained doses for correlation with the measured increases in Knoop microhardness. In-situ X-ray photoelectron spectroscopy (XPS) was performed to obtain chemical state information immediately after implantation without sputter etching or air exposure.

#### Experimental

The implantation was carried out in a unique system designed both for basic research and technical development. It consists of a 200 kV ion beam generator (supplied by Whickham Ion Beam Systems) with three beamlines, a switching magnet, quadrupole triplets, beam scanning units, a universal implantation chamber (2 x 1 m) and a Kratos XSAM 800 XPS system. The implanter is cryopumped and the ion source is diffusion pumped. Using a Freeman source, most ion species can be obtained with currents of

several milliamps. Sample temperature during implantation was usually kept below 200°C and the base pressure in the chamber as about  $1 \times 10^{-6}$  Torr, which eliminated carbon contamination problems.

Sample ABCD films (5  $\mu\text{m}$  thick) were deposited onto low carbon steel sheets (0.5 mm thick). Cut samples (1.5 cm diameter) were mounted on a target holder inside a specially designed preparation chamber which served as implantation chamber. After implantation some of the samples were transferred through a valve into the XPS chamber for analysis using MgK $\alpha$  X-rays.

Auger electron spectroscopy (AES) data were taken in a Perkin-Elmer PHI 590 system using a 5 keV primary electron beam energy and 1  $\mu\text{A}$  beam current. Depth profiling was performed using 4 keV Ar ions with a 4 x 4 mm spot size. The sputter conditions used gave a sputter rate of 57  $\text{\AA}/\text{min}$  for a tantalum oxide standard.

Surface hardness tests were performed using a Leitz microhardness tester with a Knoop diamond and an applied load of 10 g. The indentation penetrated through the implanted layers so absolute hardness values could not be determined. Nevertheless, hardening effects due to implantation could be determined in a comparative manner.

### Results and Discussion

Three different types of ABCD layers were implanted: as-deposited and annealed at 200 and 600°C. Two different implantation energies (120 and 180 keV) were used and the dose was varied from 1 to  $30 \times 10^{17} \text{ N}^+/\text{cm}^2$ . Therefore, six sets of samples were produced and analyzed. Figure 3-1 shows the AES depth profiling results obtained from the 180 keV N implanted, as-deposited ABCD layers as a function of dose. Although Cr, N, C and O were monitored during the profiling, for clarity only the Cr and N profiles are shown as atomic percent vs sputter time. Oxygen is present only in very small amounts in these films. Nitrogen displaces C during the implantation since the C profiles mimic the N profiles in an inverse manner as discussed previously [Chap 2]. In highly dosed samples,

most of the C is actually driven out of the implanted region. Based on Rutherford backscattering (RBS) and NRA data, AES overestimates the C concentration by a factor of about 2. This could be due to preferential sputtering effects or lack of accurate sensitivity factors.

The profiles in Fig. 3-1 indicate that the N concentration reaches that of Cr at a dose of about  $8 \times 10^{17} \text{ N}^+/\text{cm}^2$  and that this limiting value cannot be exceeded at higher doses. Apparently, a subsurface layer of CrN forms. At lower doses this layer broadens uniformly, but at higher doses it broadens only toward the surface. Simulation (TRIM) of 180 keV N implanted Cr containing 10 at.% C yields a maximum at a depth of 2680 Å which should coincide with the maximum in the AES N concentration profiles obtained at low dose implantation. This assumption results in a sputter etch rate of 64 Å/min. which is similar to that obtained from the Ta<sub>2</sub>O<sub>5</sub> standard. Depth profiles obtained from the other sets of samples are similar to those shown in Fig. 3-1. For 120 keV implanted samples, the implanted layers lie closer to the surface as expected and the areas under the profiles are slightly smaller due to higher sputter losses from the near-surface region during high dose implantation.

The total retained doses for implanted samples (see table 3-1) have been determined from the depth profiles by integrating the areas under the profiles using a planimeter and assuming that N losses due to sputtering are negligible at low doses ( $1-2 \times 10^{17} \text{ N}^+/\text{cm}^2$ ) since very little of the implanted N lies near the surface. Nuclear reaction analysis results support this assumption and indicate that low doses are fully retained within the error limits of the dose measurements during implantation ( $\pm 10\%$ ). Table 3-1 shows that the retained dose drops sharply after the CrN stoichiometry has been reached (doses  $> 8 \times 10^{17} \text{ N}^+/\text{cm}^2$ ). Increasing the dose from 15 to  $30 \times 10^{17} \text{ N}^+/\text{cm}^2$  introduces very little additional N into the sample. Within error limits high dose retention values for the 180 keV implanted samples are higher than those for the 120 keV implanted samples due to reduced sputter losses.

X-ray photoelectron spectroscopy spectra obtained from an as-deposited ABCD film implanted with an  $8 \times 10^{17} \text{ N}^+/\text{cm}^2$  dose of 80 keV  $\text{N}^+$  are shown in Fig. 3-2. These implantation parameters were chosen so that N was present in the near-surface region (sputter equilibrium). Three different peaks contribute to the N 1s feature. Two peaks with binding energies of 397.4 and 396.6 eV are due to  $\text{Cr}_2\text{N}$  and CrN respectively. The smaller third peak at 399.8 eV is due to molecular N trapped within the film. The C 1s peak is narrow and well defined with a binding energy of 282.6 eV indicating that essentially all of the C is present as Cr carbide but the form of this carbide is not known. The absence of hydrocarbons at the surface supports the claim that the implantation environment is clean. The predominant feature in the O 1s spectrum at 530.1 eV is due to  $\text{Cr}_2\text{O}_3$  and the asymmetry on the high binding energy side is probably due to the presence of hydroxides and adsorbed water. After sputtering for 10 min the N 1s peak shape is less defined with no peak due to molecular N remaining. The N content increases from 8 to 15 at.% and the O 1s and C 1s signals decrease slightly.

The Knoop microhardness data obtained from the six sets of samples are shown in Fig. 3-3. The values given represent an average of ten measurements. The hardness of each type of nonimplanted sample is also given. Subtraction of this value from the hardness obtained after implantation yields the hardening effect due to implantation since the irradiations were carried out below 200°C in order to minimize beam annealing effects.

For all sets of samples, the microhardness increases with N dose except for the highest dose value where a slight decrease is observed. Although the increase in hardness due to implantation appears to be small compared to that due to annealing, it is necessary to recognize the fact that the hardness measurements taken from the implanted films are problematic because the implanted layer is only a fraction of a micron thick and the hardness test probes through the Cr layer into the substrate. Thus, the hardness of the implanted layer is underestimated and the measured values shown in Fig. 3-3 should only be considered as indicators of trends.

Based on both the Auger and XPS results described above, the increase in hardness by implantation can be attributed to the formation of Cr nitrides. This assertion is supported by experiments in which Ne was implanted in as-prepared ABCD substrates using the same implantation parameters as  $N^+$ . The resulting films are softer than the as-prepared films. It seems that there is a complex relationship between nitride formation, annealing effects and structural disruption which determines the complex hardness behavior of the  $N^+$  implanted films. The decrease in hardness at the highest dose may be due to extensive structural disruptions and correlates with the formation of surface blisters which are detectable in an optical microscope. This blistering effect is less pronounced on the preannealed samples and can be suppressed by implantation at higher temperatures which allows the outward diffusion of  $N_2$  from the film.

Other experimental observations also relate to the complex relationship between nitride formation and structural disruption. Except for the as-prepared films, the films implanted with 120 keV  $N^+$  are harder than those implanted with 180 keV  $N^+$ . This fact suggests that more lattice disruption occurs in annealed (structured) films by implanting with higher energy ions. The as-prepared ABCD films are amorphous so the thicker Cr nitride layer formed by implanting with higher energy ions most likely is responsible for the increased hardness. Also, the magnitude of the nitrogen hardening effect relative to that of annealing hardening is much greater for the as-prepared films than the annealed films. This probably is due to greater structural disruption caused by implantation of the annealed films.

Initial implantation experiments on ABCD films have been carried out at an elevated sample temperature above 500°C. In this case the N retention is increased and Auger depth profiles show very broadened N distributions with diffusion tails into the bulk. The retention value is 78% for a dose of  $15 \times 10^{17} N^+/cm^2$ , a ratio of 1: 1 of N-to-Cr is not reached and hardness values greater than 3000 are obtained. Implantation of ABCD films

at elevated temperatures may lead to further improvement in the hardness and wear properties of Cr films.

Table 3-1. Retained N doses after implantation in percentage of implanted dose

Implanted dose [x 10 <sup>17</sup> ]	Unannealed		Pre-annealed 200°C		Pre-annealed 600°C	
	120 keV	180 keV	120 keV	180 keV	120 keV	180 keV
1	100	---	100	---	100	100
1.5	---	100	---	---	---	---
2	96	100	97	100	100	100
4	96	96	94	94	100	100
8	71	86	72	78	82	81
15	46	57	50	58	45	55
30	---	32	---	---	---	---

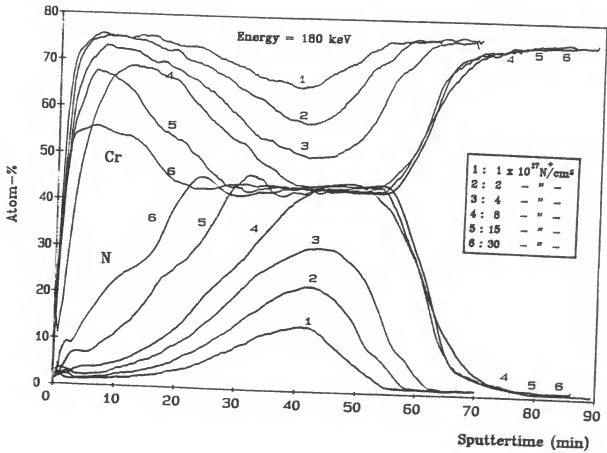


Figure 3-1. Auger depth profiles obtained from 80 keV N implanted, as deposited ABCD layers as a function of dose.



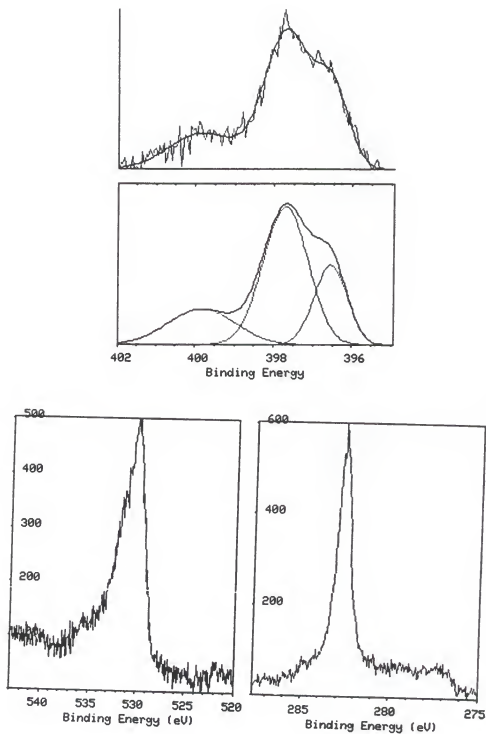


Figure 3-2. High resolution XPS data (N 1s, O 1s and C 1s features) obtained from an as-deposited ABCD film implanted with an  $8 \times 10^{17} \text{ N}^+/\text{cm}^2$  dose of 80 keV  $\text{N}^+$ . See text.

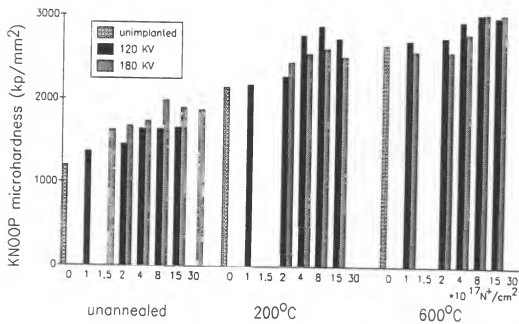


Figure 3-3. Knoop microhardness data obtained as a function of sample pretreatment, dose and implantation energy.

## CHAPTER 4

### PREPARATION AND CHARACTERIZATION STUDY OF NITROGEN-ION-IMPLANTED CONVENTIONAL CHROMIUM PLATINGS

The purpose of this chapter is to present results of a characterization study of nitrogen-implanted conventional chromium films which were obtained using electron spectroscopy for chemical analysis spectroscopy (ESCA), ion scattering spectroscopy (ISS) and AES. A related study of nitrogen-implanted ABCD films will also be discussed [Chap 5]. The ultimate goals of these studies are to prepare chromium layers with improved properties and to understand the relationships between mechanical properties, chemical behavior and microstructural properties of these films.

#### Experimental

The conventional chromium layers were prepared by electrodepositing chromium from a solution containing  $250 \text{ g l}^{-1}$  of chromic acid and  $2.5 \text{ g l}^{-1}$  of sulfuric acid at a temperature of  $50^\circ\text{C}$  and a current density of  $40 \text{ A dm}^{-2}$  for 30 min. After deposition the samples were ultrasonically cleaned in acetone and ethanol and then annealed at  $600^\circ\text{C}$  in a mechanically roughed  $10^{-5}$  Torr vacuum for 1/2 h. Annealing in such a hydrocarbon background is known to increase the carbon content of these chromium layers [8]. Next, the chromium samples were  $\text{N}^+$  implanted using  $90 \text{ keV N}^+$ . The ion flux was kept low in order to minimize heating effects during implantation and it is believed that the sample temperature remained beneath  $250^\circ\text{C}$ . The total dose used was  $1 \times 10^{18} \text{ N}^+/\text{cm}^2$ .

Auger electron spectroscopy, ESCA, and ISS were performed using a double-pass cylindrical mirror analyzer (CMA) (PHI model 25-270 AR) contained in a vacuum system with a base pressure of  $5 \times 10^{-11}$  Torr. Auger electron spectroscopy data were obtained by using a primary beam energy of  $3 \text{ keV}$ . The CMA was operated in the non-retarding mode

with a peak-to-peak oscillation voltage of 0.5 V and a 5 kHz frequency. A 20  $\mu\text{A}$  primary beam current was focused to a spot approximately 0.5 mm in diameter. ESCA data were taken in the retarding mode with a pass energy of 50 eV using a computer-interfaced, digital, pulse-counting circuit [15] and digital filtering techniques [16]. Utilization of smaller pass energies does not result in significantly increased resolution. Also, the conditions used to collect AES and ESCA spectra result in negligible damage to the surface. Ion scattering spectroscopy was carried out in the non-retarding mode using a defocused primary beam of 1 keV  $^4\text{He}$  ions (100 nA over an area 1 cm in diameter for 1 min). A small ISS primary beam flux was used in order to minimize beam damage. Primary-beam-induced damage was negligible since ISS spectra taken repeatedly show essentially no differences. Ion sputtering was performed using a sputter gun system (PHI model 04-161) to produce an argon ion beam of 0.5 keV and 2  $\mu\text{A}$  over a spot diameter of approximately 1 cm. Charging did not occur in the application of any of these techniques to samples examined in this study.

### Results and Discussion

Figure 4-1 shows Auger spectra taken from the annealed and  $\text{N}^+$ -implanted conventional chromium sample before  $\text{Ar}^+$  ion sputtering (spectrum a), after sputtering for 135 min (spectrum b) and after sputtering for 240 min (spectrum c). Spectrum a exhibits very large carbon and oxygen peaks, smaller chromium peaks and a small nitrogen peak. The shape of the carbon peak indicates that the carbon may be due to a graphitic form or more likely due to the presence of adsorbed hydrocarbons. The Auger sensitivity factor of carbon is quite low [17] so a large amount of carbon is present on the surface after implantation. This carbon probably accumulated on the surface during annealing, air exposure and implantation. Auger spectra taken from conventional chromium films normally exhibit features due to sulfur, chlorine, calcium and potassium. The sulfur peak appears as a result of the utilization of a sulfate catalyst for the electrodeposition, and the

other species are contaminants in the bath. However, peaks due to these species are not present in spectrum a either because they are covered by the carbon or because they were sputtered off the surface during implantation.

Auger compositional profile data are shown in Fig. 4-2. The compositional information was calculated using published sensitivity factors [17] and peak-to-peak heights obtained from Auger spectra taken intermittently during sputtering. This approach neglects many important factors which influence quantification such as peak shape change as a function of chemical state and matrix effects so the profiles in Fig. 4-2 should be considered to be semiquantitative. Also, the sputter rate is not known and is probably quite low. A crude estimate would be about 30 Å per 100 min. The profiles show that the layer examined contains a large amount of oxygen and that the O:Cr ratio decreases with sputtering. The near-surface region consists of a carbon-rich layer, and the carbon concentration below that region remains quite high. The nitrogen concentration monotonically increases with depth as does the chromium concentration. The sulfur concentration is low throughout the region investigated but increases slightly as the carbon-rich layer is sputtered away. An interesting change occurs with sputtering from 220 to 250 min. The nitrogen and chromium concentrations increase rather sharply while the carbon concentration decreases sharply indicating that implanted nitrogen displaces carbon from the implanted region as observed previously [Chap. 2].

The compositional trends discussed with regard to the profiles in Fig. 4-2 can also be observed in the Auger spectra b and c shown in Fig. 4-1 taken after sputtering for 135 min and 240 min respectively. An argon peak also appears as a result of sputtering. In addition to compositional trends, significant peak shape changes are observed, particularly for the carbon and chromium peaks. The carbon peak shape obtained after sputtering suggests that the hydrocarbon-type carbon is still present and that at least one other form of carbon is present. Unfortunately, the carbon peak shape is complex, making it difficult to extract more information. The chromium peak shape change is indicative of the presence of

larger amounts of metallic chromium beneath the surface which is consistent with the fact that the O:Cr concentration ratio decreases with increasing sputter time. The carbon and chromium chemical states as a function of depth are discussed further in conjunction with the ESCA data presented below.

Ion scattering spectroscopy (ISS) spectra taken from the sample before and after sputtering for 240 min are shown in Fig. 4-3, spectra a and b respectively. Since ISS is essentially sensitive only to the outermost atomic layer, it is not surprising that a distinct peak due to chromium does not appear in the spectrum obtained from the surface before sputtering. The large low  $E/E_0$  feature is due mostly to carbon and nitrogen, and the asymmetry on the high  $E/E_0$  side is due to oxygen. The region between  $E/E_0$  values of 0.5 and 0.75 exhibits noise and a decreasing signal. This structure is probably due to subsurface (maybe second layer) sulfur and chromium. The ISS spectrum taken after sputtering shown in Fig. 4-3, spectrum b, is considerably different from that taken before sputtering. The oxygen and chromium features are now prominent. The carbon feature is quite small, and the nitrogen yields a shoulder on the oxygen peak. The large inelastic background on the low kinetic energy sides of the oxygen and chromium features indicates that the surface has a non-metallic nature [18]. A very small peak appears at  $E/E_0 = 0.87$ . This peak may be due to double scattering events.

X-ray photoelectron spectroscopy (XPS or ESCA) survey spectra taken from the sample before and after sputtering for 240 min are shown in Fig. 4-4, spectra a and b respectively. These data are consistent with the Auger depth profiling data in that the as-prepared surface exhibits a predominant carbon peak, a very small nitrogen peak and a large O:Cr peak height ratio. After sputtering, the carbon peak is greatly decreased with respect to the chromium features, the nitrogen peak is increased and the O:Cr peak height ratio is decreased. However, peaks due to sulfur are not discernible, but this is not unexpected since the ESCA sulfur sensitivity factor is quite low [19] whereas its AES

sensitivity factor is large [17], resulting in a significant feature in the Auger spectra shown in Fig. 4-1, spectra b and c.

Significant changes with depth are observed in the high resolution ESCA chromium, oxygen, carbon and nitrogen features shown in Figs. 4-5, 4-6, 4-7 and 4-8 respectively. The peaks in these figures have all been normalized to about the same size to allow for comparison of the peak shapes.

The chromium peak shapes shown in Fig. 4-5 are quite complex both before and after sputtering. Before sputtering most of the chromium is in an oxidic form, but a large shoulder due to metallic chromium is present on the low binding energy side. The chromium oxides present are probably a mixture of  $\text{CrO}_3$ ,  $\text{Cr}_2\text{O}_3$ ,  $\text{CrO}_2$  and chromium hydroxides. After sputtering, chromium is present predominantly as a nitride and in metallic form. The shoulder on the high binding energy side is due to the presence of  $\text{Cr}_2\text{S}_3$  and several different oxides including  $\text{Cr}_2\text{O}_3$ ,  $\text{CrO}_3$  and  $\text{CrO}_2$ .

Corresponding changes are also observed in the ESCA O 1s peaks shown in Fig. 4-6. Before sputtering the O 1s peak is very broad and exhibits shoulders indicating the presence of multiple chemical states of oxygen. The higher binding energy shoulder on this peak is probably due to the presence of hydroxyl groups and adsorbed water as discussed previously [8]. Sputtering removes most of these species causing the O 1s peak to become narrow and characteristic of oxygen present in the form of chromium oxides.

Even larger deviations with sputtering are found in the ESCA C 1s spectra shown in Fig. 4-7. The large peak obtained from the surface before sputtering (spectrum a) is symmetrical with a binding energy of 284.7 eV. This is characteristic of carbon bound as hydrocarbon-like or graphitic species, and the symmetry suggests that other carbon chemical states are not present in the carbon overlayer. However, after sputtering for 240 min, many carbon chemical states are present as observed in spectrum b. The carbon peak is greatly decreased in size by sputtering (see Fig. 4-4), but spectrum b has been expanded in the y direction to allow for a comparison of the peak shape with the spectrum in Fig. 4-

7(a). It appears that at least seven different carbon chemical states with binding energies of 281.8, 282.3, 284.0, 284.4, 285.7, 286.4 and 287.7 eV contribute to the C 1s feature. The assignment of these states is difficult and cannot be done unambiguously. The peaks at 281.8 and 282.3 eV are due to chromium carbide. However, since there are at least two chromium carbides ( $\text{Cr}_7\text{C}_3$  and  $\text{Cr}_{23}\text{C}_6$ ) and the binding energies of the C 1s level in these compounds are not known, it is not possible to specify the form of the carbide. The peak at 284.0 eV also has a binding energy lower than those of most carbon compounds [19] and, therefore, may be due to some form of chromium carbide. The peak at 284.4 eV may be due to hydrocarbons which have been altered by ion bombardment. The nitrogen ions which strike the surface are highly energetic and reactive so they may react with substrate carbon to form some type of C-N species. The shoulder at 285.7 eV may be due to a species such as  $\text{MeCH}_2\text{NH}_2$  which is known to yield this C 1s binding energy [19]. Another shoulder appears at 286.4 eV which could be due to another C-N type of species. A small high binding energy peak appears at 287.7 eV which is probably due to adsorbed CO. These peaks appear in varying ratios after sputtering for different periods of time.

The N 1s peaks are shown in Fig. 4-8. Three assignment lines have been drawn in this figure which correspond to CrN at 396.6 eV,  $\text{Cr}_2\text{N}$  at 397.4 eV, and molecular nitrogen at 399.8 eV 1s. Before sputtering, the N 1s, peak is small and broad, indicating that both CrN and  $\text{Cr}_2\text{N}$  are present at the surface. After sputtering, CrN is the predominant form of nitride present, and a shoulder due to molecular nitrogen appears. This  $\text{N}_2$  probably is trapped in lattice imperfections which may have formed during the implantation. Other forms of nitrogen may also be present such as the C-N species discussed above.

X-ray photoelectron spectroscopy (XPS or ESCA), ISS and AES coupled with sputter depth profiling have been used in this study to examine the chemical nature of nitrogen-ion-implanted conventional chromium films. The data indicate that both the composition and chemical state of the species in the near-surface region are a strong



function of depth. The outermost 10Å consists of a carbon-rich layer which appears to be due to adsorbed hydrocarbons. The carbon concentration decreases as the nitrogen concentration increases with depth, and several carbon species including chromium carbides are present beneath the surface. The ISS data show that the outermost atomic layer consists of carbon and nitrogen and that carbon, nitrogen, oxygen and chromium lie beneath the surface. The chemical state of the chromium changes from oxidic at the surface to primarily metallic and nitridic beneath the surface. The nitrogen is present as CrN and Cr<sub>2</sub>N at the surface and predominantly as CrN and N<sub>2</sub> beneath the surface. Because of the complex chemical nature of this surface, it is difficult to determine which factors contribute to the increase in hardness during implantation. However, the presence of chromium nitride and carbide phases must contribute in some manner to the increased hardness.

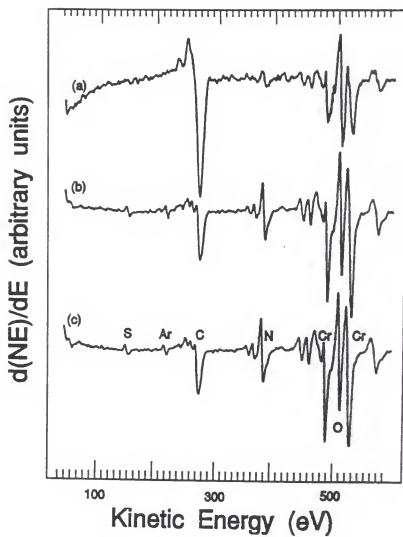


Figure 4-1. Auger spectra taken from the as-prepared, annealed and implanted conventional chromium sample (spectrum a), after ion sputtering for 135 min (spectrum b) and after ion sputtering for 240 min (spectrum c).

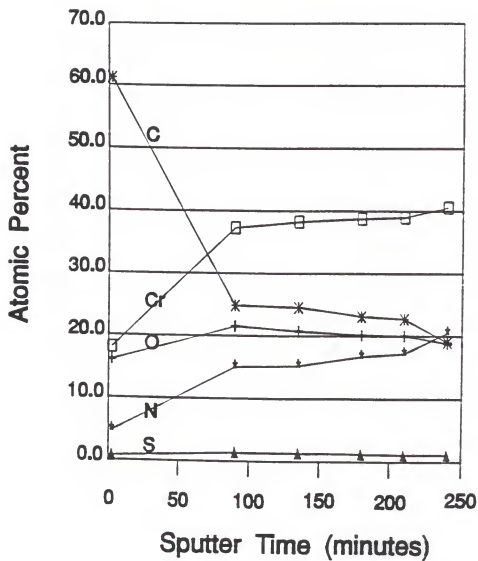


Figure 4-2. Auger composition (atomic per cent) depth profiles shown as a function of sputter time.

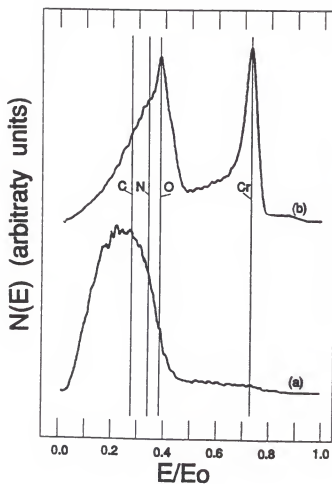


Figure 4-3. Ion scattering spectroscopy spectra taken from the as-prepared annealed and implanted conventional chromium sample before (spectrum a) and after (spectrum b) sputtering for 240 min.

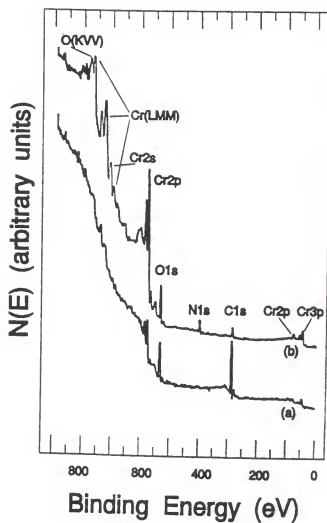


Figure 4-4. X-ray photoelectron spectroscopy (XPS or ESCA) spectra taken from the as-prepared, annealed and implanted conventional chromium sample before (spectrum a) and after (spectrum b) sputtering for 240 min.

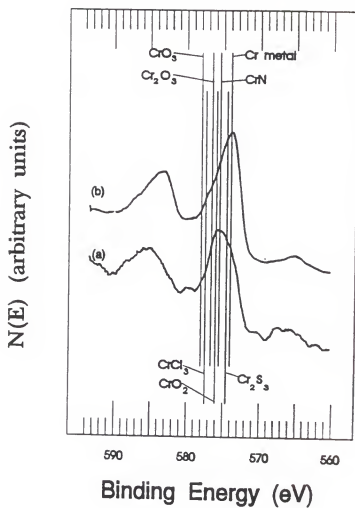


Figure 4-5. High resolution ESCA Cr 2p features obtained before (spectrum a) and after (spectrum b) sputtering for 240 min.

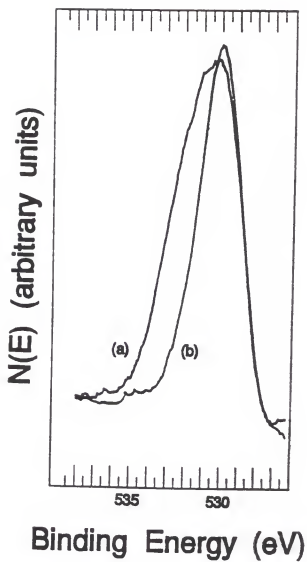


Figure 4-6. High resolution O 1s spectra taken before (spectrum a) and after (spectrum b) sputtering for 240 min.

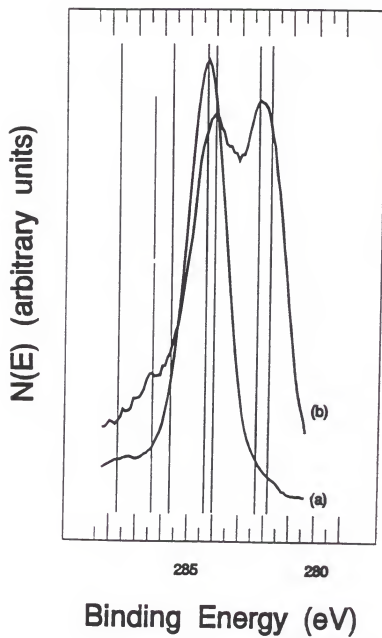


Figure 4-7. High resolution C 1s spectra taken before (spectrum a) and after (spectrum b) sputtering for 240 min.



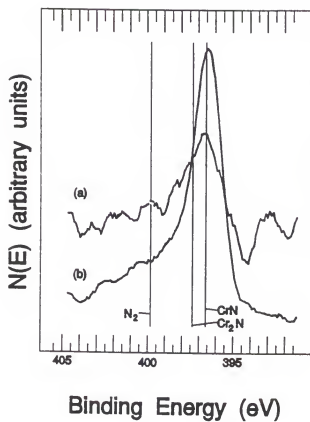


Figure 4-8. High resolution N 1s spectra taken before (spectrum a) and after (spectrum b) sputtering for 240 min.

## CHAPTER 5

### CHARACTERIZATION STUDY OF NITROGEN-ION-IMPLANTED AMORPHOUS BRIGHT CHROMIUM DEPOSITED FILM

The purpose of this present chapter is to characterize a nonannealed and a preannealed  $N^+$ -implanted ABCD film using Auger electron spectroscopy (AES), electron spectroscopy for chemical analysis (ESCA or XPS) and X-ray diffraction (XRD). Information was obtained which is useful in understanding the relationship between hardness, chemical composition of the films and structure.

#### Experimental

The method of preparation of the ABCD films used in this study has been described previously [3]. One film was not preannealed, and the other was preannealed at 600°C for 1 hour in UHV. Both films were implanted using 120 keV  $N^+$  at a total dose of  $1.5 \times 10^{18}$  ions/cm<sup>2</sup> using a mass analyzed beam and a current density of about 40 mA/cm<sup>2</sup> which resulted in a sample temperature below 200°C during implantation. Compositional depth profiles of  $N^+$  implanted ABCD films using AES have been published in previous studies [Chap. 2, Chap. 3]. The results indicate that about 45% of the dose is retained in each of the films. The loss mechanism is most likely preferential sputtering of back-diffused N from the surface. The N loss becomes more pronounced after completion of the subsurface CrN layer (dose  $> 8 \times 10^{17}$   $N^+$ /cm<sup>2</sup>). The diffusion of N out of the implanted layer toward the surface is facilitated by the high defect density near the surface. The calibrated Auger depth profiles are probably accurate to  $\pm 5\%$ . The experimental details regarding AES and ESCA have been described previously [Chap. 4] and are not reproduced here. The difference in Knoop microhardness (obtained using a 0.1 N load) is quite large, 1660 for the nonannealed film and 2980 for the annealed film. These ABCD films have a Knoop

microhardness of about 800 before implantation. This difference is due only to the fact that one sample was preannealed.

### Results and Discussion

Auger spectra taken from the near-surface regions of the nonannealed and annealed samples are shown in Fig. 5-1(a) and (b) respectively. Peaks due to Cr, O, C and N are present in these spectra, and the compositions are quite similar based on the relative sizes of the peaks. These spectra indicate that the surface layer is oxide in nature and contains a relatively small amount of N. The shape of the C peaks indicate that it is adsorbed hydrocarbons or of graphitic form.

Auger spectra obtained from the bulk of the implanted regions of the (a) nonannealed and (b) annealed are shown in Fig. 5-2. In order to obtain these spectra, about 40 nm of the outermost surface was ion sputtered away using 1 keV Ar<sup>+</sup> ions. Again, the spectra are quite similar with regard to relative peak heights except that the bulk region of the annealed samples is enriched in O. This is most likely due to migration of O from the oxide overlayer into the bulk during annealing [6,8]. Another difference between the two spectra is the shape of the C peak. The C peak shape in the spectrum obtained from the nonannealed sample is due to a mixture of C chemical states since no single state has a peak shape of this type. The C peak shape in the spectrum obtained from the annealed samples has a carbidic shape, but it also can be due to a mixture of more than one chemical state. This is discussed in more detail below with regard to the C 1s ESCA spectra.

The Cr 2p ESCA spectra obtained from the samples before ((a) and (b)) and after sputtering ((c) and (d)) are shown in Fig. 5-3. The spectra taken from the (a) nonannealed and (b) annealed surfaces before sputtering are similar and characteristic of spectra obtained from an oxide overlayer. The Cr is predominantly in the form of Cr<sub>2</sub>O<sub>3</sub>, but other chemical forms including CrO<sub>3</sub>, CrO<sub>2</sub>, nitrides and Cr metal are present to some extent. Shoulders

due to CrN are apparent. Spectra obtained after sputtering are shown in (c) for the nonannealed sample and (d) for the annealed sample. The primary Cr chemical state is metallic, but there is a distinct asymmetry and broadening to the high binding energy side due to the presence of nitrides and oxides. A pronounced shoulder due to these species is present on the spectrum obtained from the annealed sample. Based on the Auger spectra shown in Fig. 5-2, a large amount of C is present in this region. Unfortunately, Cr 2p binding energies for Cr carbides are not available in the ESCA literature so a more detailed interpretation of the spectra shown in Fig. 5-3(c) and (d) is not possible.

Carbon 1s spectra corresponding to the Cr 2p spectra shown in Fig. 5-3 are shown in Fig. 5-4. The C 1s spectra taken from the (a) nonannealed and (b) annealed surfaces before sputtering exhibit a predominant peak which is due to graphitic C or adsorbed hydrocarbons. This is consistent with the Auger data shown in Fig. 5-1. Shoulders with high binding energies (287 to 291 eV) are also present. These are probably due to hydrocarbons which contain both N and O. The shapes of the C 1s peaks obtained from the bulk of the implanted regions of the (c) nonannealed and (d) annealed samples are very different from those shown in (a) and (b) and from each other. The predominant peak in both (c) and (d) is designated a carbide and based on the XRD data described below is probably due to  $\text{Cr}_7\text{Cr}_3$ . Another form of carbide  $\text{Cr}_3\text{C}_2$  may also be contributing to these spectra. A large shoulder is present on the high binding energy side of the carbide peak in both spectra, but the chemical state of the C responsible for this shoulder is not known. Its relative intensity compared to the carbide peak is greater for the nonannealed sample which suggests that annealing converts this form of C into carbide ( $\text{Cr}_7\text{C}_3$ ). Other chemical forms of C are probably present in small amounts.

Nitrogen 1s ESCA spectra corresponding to the Cr 2p and C 1s ESCA spectra shown in Figs. 5-3 and 5-4 respectively are shown in Fig. 5-5. The N 1s spectra obtained from the (a) nonannealed and (b) annealed samples before sputtering exhibit a low signal-to-noise ratio which suggest that very little N is present in the near-surface region. This is

consistent with the Auger data shown in Fig. 5-1. Several chemical forms of N are present at these surfaces including CrN, possibly  $\text{Cr}_2\text{N}$ , [20] organic compounds containing N and perhaps small amounts of  $\text{NH}_4^+$  and  $\text{N}_2$ . Nitrogen 1s spectra taken from the (c) nonannealed and (d) annealed surfaces after sputtering into the bulk implanted region are similar to each other in both size and shape. This fact indicates that preannealing an ABCD layer does not influence the amount or chemical form of N resulting from implantation. The predominant peak is due mostly to CrN probably with a small contribution from  $\text{Cr}_2\text{N}$ . A distinct shoulder appears which is probably due to some C and N-containing compound.

X-ray diffraction data taken from the (a) annealed and (b) nonannealed samples are shown in Fig. 5-6. The pattern obtained from the nonannealed sample indicates little structure which is primarily due to  $\text{Cr}_2\text{N}$  [21] and a very small amount of  $\text{Cr}_7\text{C}_3$ . Also, some crystalline Cr metal may be present. The nonimplanted, as-prepared ABCD films are amorphous [3] the structure apparent in Fig. 5-6(b) is due to the implantation process. Some annealing at temperatures below  $250^\circ\text{C}$  occurs during implantation which would cause an increase in the crystallinity. As expected, the annealed sample is highly crystalline and exhibits features due to metallic Cr,  $\text{Cr}_2\text{N}$  and  $\text{Cr}_7\text{C}_3$ . The ESCA and AES data cannot be compared directly with the XRD data because XRD is a bulk-sensitive technique. Nevertheless, some relationships can be drawn. Certainly, the  $\text{Cr}_2\text{N}$  found in the XRD patterns contribute to the N 1s ESCA spectra in Fig. 5-5. The facts that diffraction peaks due to CrN are not observed in XRD but that a strong ESCA N 1s feature due to CrN is observed suggests that CrN remains in a noncrystalline form under the conditions utilized in this study. Also, the  $\text{Cr}_7\text{C}_3$  found in XRD contributes to the C 1s ESCA spectrum in Fig. 5-4(c) and (d).

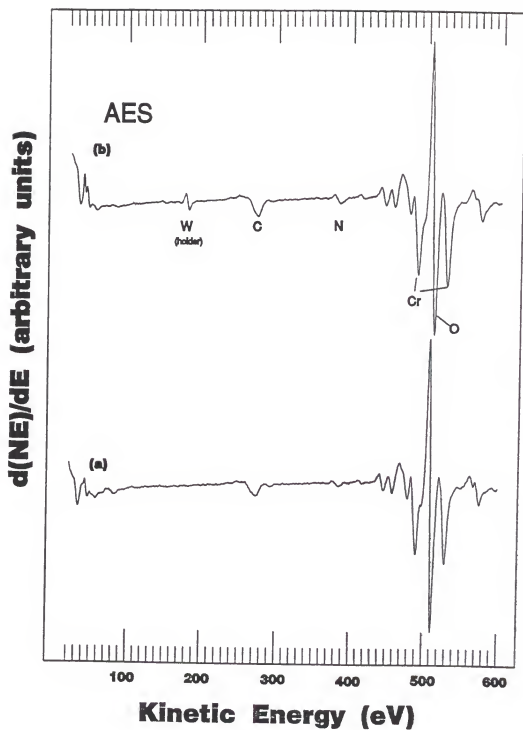


Figure 5-1. Auger spectra taken from the near-surface regions of the (a) nonannealed and (b) annealed ABCD films. The W in spectrum (b) originates from the sample holder.

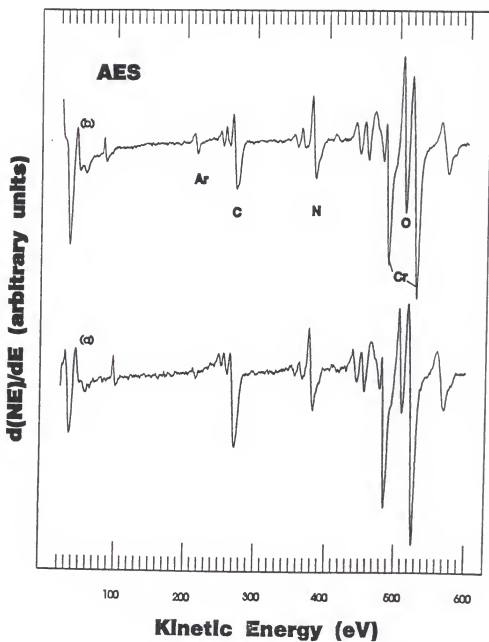


Figure 5-2. Auger spectra taken from the bulk of the implanted regions of the (a) nonannealed and (b) annealed ABCD films.

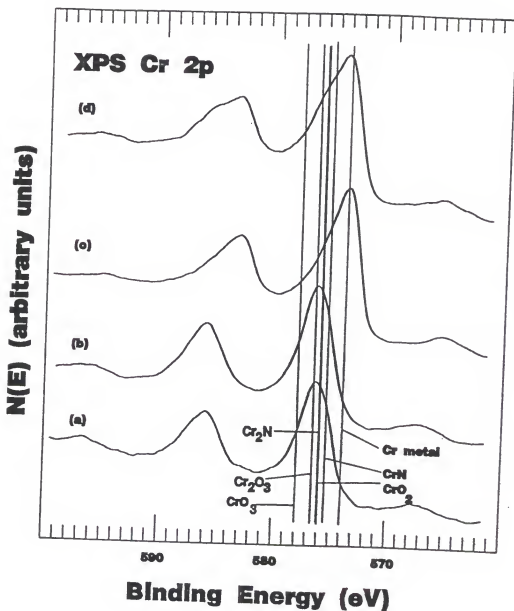


Figure 5-3. Chromium 2p ESCA spectra obtained from (a) nonannealed and (b) annealed surfaces before sputtering and the (c) nonannealed and (d) annealed surfaces after sputtering.



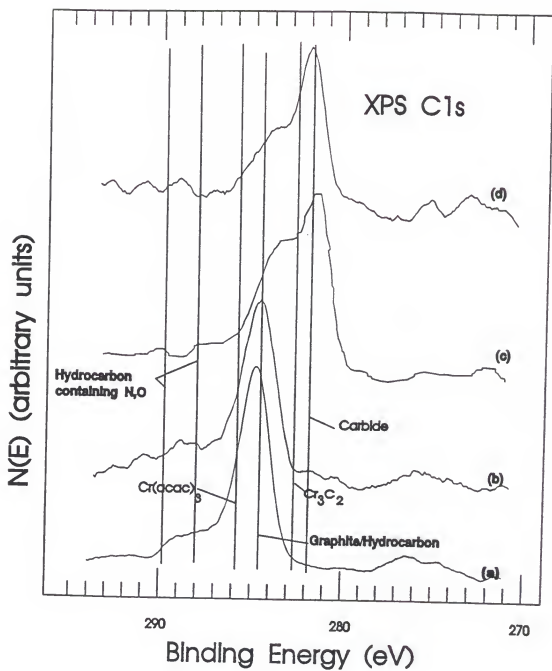


Figure 5-4. Carbon 1s ESCA spectra obtained from the (a) nonannealed and (b) annealed surfaces before sputtering and the (c) nonannealed and (d) annealed surfaces after sputtering.

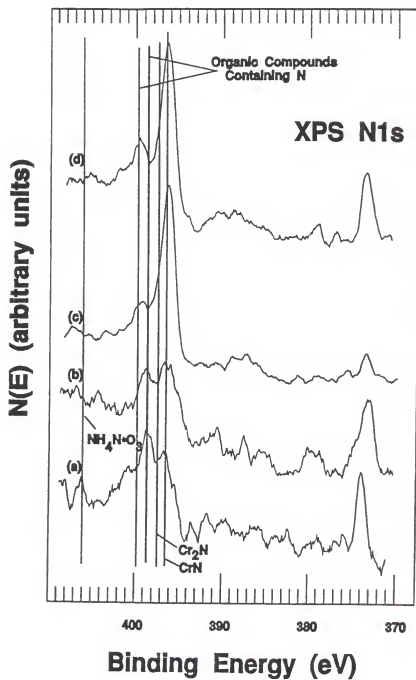


Figure 5-5. Nitrogen 1s ESCA spectra obtained from the (a) nonannealed and (b) annealed surfaces before sputtering and the (c) nonannealed and (d) annealed surfaces after sputtering.

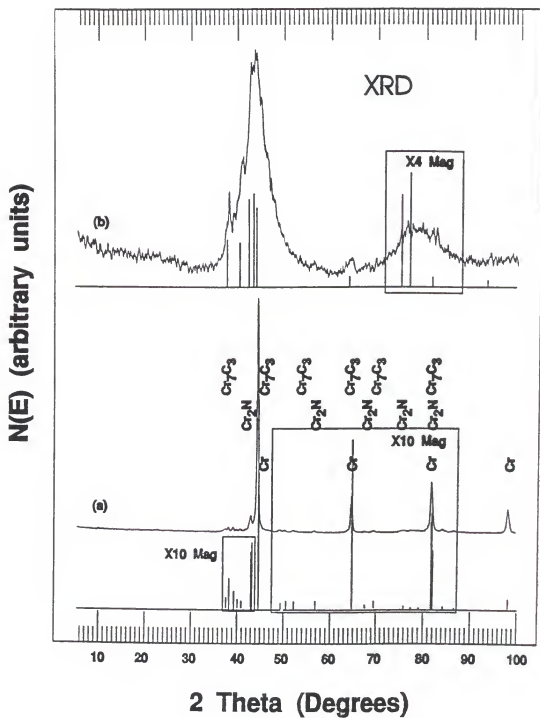


Figure 5-6. X-ray diffraction data obtained from the (a) annealed and (b) nonannealed samples.

## CHAPTER 6 CONCLUSION

### Summary and Conclusion

Nitrogen-ion implantation of conventional Cr and amorphous bright chromium-deposited (ABCD) films, which were preannealed at various temperatures, has been carried out in order to determine the effect of implantation on the hardness of the Cr layers. The implantation was carried out using low ion beam fluxes in order to maintain a sample temperature below 250°C. Implantation leads to increased hardness, but the extent is most pronounced for conventional films which were not annealed and ABCD films which were annealed at or below 400°C for 1/2 h. The surface sensitivity of the hardness measurements was varied by altering the load used during the test. Data obtained in this manner show that the more surface-sensitive hardness is greater than the more bulk-sensitive hardness for both the implanted and non-implanted ABCD films and the implanted conventional Cr films. The compositions of the implanted films have been characterized using Auger electron spectroscopy in conjunction with sputter depth profiling. These data show that all of the Cr in the implanted region is bound as CrN, Cr oxides and Cr carbides at large total N<sup>+</sup> doses. Furthermore, the N displaces the C in ABCD films producing N and C profiles that mimic each other in an inverse manner.

Since the hardness of amorphous bright chromium deposited (ABCD) layers can be increased by annealing or N<sup>+</sup> implantation. The N<sup>+</sup> implantation parameters which influence hardness have been systematically examined. These parameters include sample pretreatment, ion beam energy and total dose. The properties of the resulting films have been characterized using AES coupled with ion sputtering depth profiling, XPS (or ESCA) and Knoop microhardness measurements. Auger depth profiles suggest the formation of a stoichiometric CrN subsurface layer after implantation of high N doses ( $> 8 \times 10^{17}$

$\text{N}^+/\text{cm}^2$ ). With higher doses this layer broadens toward the surface and N retention values decrease rapidly. Implanting at elevated temperatures increases the retained N, causes N to migrate more deeply into the bulk, and yields high hardness values.

The complex chemical nature of  $\text{N}^+$ -implanted conventional chromium films using ESCA (or XPS), AES, depth profiling and ISS. Both the composition and chemical states of the species vary substantially with depth, and numerous forms of chromium, carbon, nitrogen and oxygen are present.

The effect of annealing ABCD  $\text{N}^+$ -implanted films was also examined. A non-annealed film and a  $600^\circ\text{C}$  annealed film were implanted with nitrogen ions and characterized using Auger electron spectroscopy (AES), electron spectroscopy for chemical analysis (ESCA or XPS) and X-ray diffraction (XRD). The resulting data yield information which relates the hardness of the films to their chemical and structural properties. Specifically, the annealed film is more highly crystalline than the non-annealed film. Diffraction lines due to  $\text{Cr}_7\text{C}_3$  and  $\text{Cr}_2\text{N}$  are readily apparent. Auger electron spectroscopy and ESCA show that the film compositions are similar but that the chemical states of the surface species differ in that most of the organic carbon contained in the film is converted to carbide during annealing. These differences are responsible for the increase in Knoop hardness (1660 to 2980) derived from annealing the sample prior to implantation.

Pre-annealing an ABCD film before  $\text{N}^+$  implantation has a large effect on its hardness. The ESCA, AES and XRD data show that this increase in hardness is due to an enhanced crystallinity caused by annealing and the formation of  $\text{Cr}_7\text{C}_3$  during annealing. The  $\text{N}^+$  implantation process itself apparently is not affected by the preannealing step.

#### Future Investigations

The body of work presented here is the foundation for further investigation of the incorporation of N species into ABCD films. The final goal of these investigations is to be

able to produce an ABCD film that is specifically tailored for an application. This not only requires controlling the hardness, but the structure and chemical properties as well.

Since the incorporation of N species into ABCD films with ion implantation gives increased hardness, addition of N species through the bath constituents should also be investigated. A subsequent energy based treatment to overcome the activation energy required to form the desired N species and structures associated with increased hardness will be required. This energy based treatment may be thermal, electrical or possibly mechanical. The treatment would have to be uniform over the depth of the film as the desired goal for this treatment is to produce an ABCD film with uniformly increased hardness.

Improvements to the surface properties of the films could also be enhanced by exposure to a flux of hyperthermal neutral atoms. Oxygen-atom exposure could produce a very uniform oxide surface coating of ABCD films with an increased resistance to corrosion by reducing the sites for chemical attack on the film surface. Hydrogen-atom exposure could produce a clean, oxide free surface that could be subsequently exposed to a N-atom flux to produce a very hard, uniform, nitridic surface.

## REFERENCES

1. G. J. Sargent, *Trans. Am. Electrochem. Soc.*, 37, 479 (1920).
2. C. G. Fink, US Patent 1,581,188 (1926).
3. S. Hoshino, H. A. Laitinen and G. B. Hoflund, *J. Electrochem. Soc.* 133, 681 (1986).
4. S. Hofmeister, G. B. Hoflund, C. K. Mount, S. Hoshino and H. Ferber, to be published.
5. Y. Nonaka, K. Saito, T. Inoue and S. Hoshino, extended abstract, 79th Annual Conference of the Surface Finishing Soc. of Japan, p. 172 (1989).
6. G. B. Hoflund, D. A. Asbury, S. J. Babb, A. L. Grogan, Jr., H. A. Laitinen and S. Hoshino, *J. Vac. Sci. Technol. A4*, 26 (1986).
7. G. B. Hoflund, A. L. Grogan, Jr., D. A. Asbury, H. A. Laitiner and S. Hoshino, *Appl. Surf. Sci.* 28, 224 (1987).
8. G. B. Hoflund, M. R. Davidson, E. Yngvadottir, H. A. Laitinen and S. Hoshino, *Chem. Mater.* 1, 625 (1989).
9. R.-Y. Tsai and S.-T. Wu, *J. Electrochem. Soc.* 136 (1989) 1341.
10. G.D. Lempert, *Surf. Coat Technol.* 34 (1988) 185.
11. K. Terashima, T. Minegishi, M. Iwaki and K. Kawashima, *Mater. Sci. Eng.* 90 (1987) 229.
12. T. Fujihana, Y. Okabe and M. Iwaki, *Mater. Sci. Eng. A115* (1989) 291.
13. E. Broszeit, H.J. Schroder and G.K. Wolf, *Z. Werkstoff-tech.* 18 (1987) 356.
14. D. J. Siconolfi and R. P. Frankenthal, *Corros. Sci.* 24, 137 (1984).
15. R. E. Gilbert, D. F. Cox and G. B. Hoflund, *Rev. Sci. Instrum.*, 53 (1982) 1281.
16. A. Savitsky and M. J. E. Golay, *Anal. Chem.*, 36 (1984) 1627.
17. L. E. Davis, N. C. MacDonald, P. W. Palmberg, G. E. Riach and R. E. Weber, *Handbook of Auger Electron Spectroscopy*, Physical Electronics Industries, Eden Prairie, MN, 1976.
18. S. D. Gardner, G. B. Hoflund, M. R. Davidson and D. R. Schryer, *J. Catal.*, 115 (1989) 132.

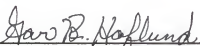
19. C. D. Wagner, W. M. Riggs, L. E. Davis, J. F. Moulder and G. E. Muilenberg, *Handbook of X-ray Photoelectron Spectroscopy*, Perkin-Elmer, Eden Prairie, MN, 1979.
20. M. Romand and M. Roubin, *Analysis*, 4, (1976) 309.
21. D. Wang and T. Oki, *Thin Solid Films*, 185, (1990) 219.



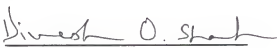
### BIOGRAPHICAL SKETCH

Charles Kohler Mount was born in Springfield, Massachusetts. He graduated from Rensselaer Polytechnic Institute with a degree in chemistry. After several years in the U.S. Navy, he is now pursuing a career of scientific research.

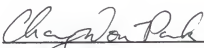
I certify that I have read this study and that in my opinion it conforms to acceptable standards of scholarly presentation and is fully adequate, in scope and quality, as a dissertation for the degree of Doctor of Philosophy.

  
Gar B. Hoflund, Chairman  
Professor of Chemical Engineering

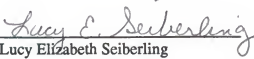
I certify that I have read this study and that in my opinion it conforms to acceptable standards of scholarly presentation and is fully adequate, in scope and quality, as a dissertation for the degree of Doctor of Philosophy.

  
Dinesh O. Shah  
Professor of Chemical Engineering

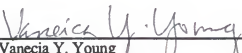
I certify that I have read this study and that in my opinion it conforms to acceptable standards of scholarly presentation and is fully adequate, in scope and quality, as a dissertation for the degree of Doctor of Philosophy.

  
Chang-Won Park  
Associate Professor of Chemical  
Engineering

I certify that I have read this study and that in my opinion it conforms to acceptable standards of scholarly presentation and is fully adequate, in scope and quality, as a dissertation for the degree of Doctor of Philosophy.

  
Lucy Elizabeth Seiberling  
Professor of Physics

I certify that I have read this study and that in my opinion it conforms to acceptable standards of scholarly presentation and is fully adequate, in scope and quality, as a dissertation for the degree of Doctor of Philosophy.

  
\_\_\_\_\_  
Vanecia Y. Young  
Associate Professor of Chemistry

This dissertation was submitted to the Graduate Faculty of the College of Engineering and to the Graduate School and was accepted as partial fulfillment of the requirements for the degree of Doctor of Philosophy.

December, 1997

  
\_\_\_\_\_  
Winfred M. Phillips  
Dean, College of Engineering

\_\_\_\_\_  
Karen A. Holbrook  
Dean, Graduate School